

Surgical Foundation Model Leveraging Compression and Entropy Maximization for Image-Guided Surgical Assistance

Lianhao Yin^{1,2}, Ozanan Meireles^{1,4}, Guy Rosman^{1,4}, Daniela Rus²

Abstract—Real-time video understanding is critical to guide procedures in minimally invasive surgery (MIS). However, supervised learning approaches require large, annotated datasets that are scarce due to annotation efforts that are prohibitive, e.g., in medical fields. Although self-supervision methods can address such limitations, current self-supervised methods often fail to capture structural and physical information in a form that generalizes across tasks. We propose Compress-to-Explore (C2E), a novel self-supervised framework that leverages Kolmogorov complexity to learn compact, informative representations from surgical videos. C2E uses entropy-maximizing decoders to compress images while preserving clinically relevant details, improving encoder performance without labeled data. Trained on large-scale unlabeled surgical datasets, C2E demonstrates strong generalization across a variety of surgical ML tasks, such as workflow classification, tool-tissue interaction classification, segmentation, and diagnosis tasks, providing improved performance as a surgical visual foundation model. As we further show in the paper, the model’s internal compact representation better disentangles features from different structural parts of images. The resulting performance improvements highlight the yet untapped potential of self-supervised learning to enhance surgical AI and improve outcomes in MIS.

Index Terms—Foundation model, Information compression, Self-supervised learning, Minimum invasive surgery, Surgical videos

I. INTRODUCTION

Artificial intelligence-enabled video analysis and minimally invasive surgery (MIS) are revolutionizing surgical practices, enhancing patient outcomes in multiple tasks throughout the preoperative, intraoperative, and postoperative surgical lifecycle. AI algorithms significantly improve preoperative planning by accurately segmenting medical images, reducing surgical errors, and optimizing resource allocation [1], [2]. In the surgical intraoperative setting, computer vision approaches can

help evaluate the difficulty of surgery, guide safe dissection, improve staff awareness and readiness in real time by detecting tools, tissues, workflow stages, and performing tissue segmentation [3]–[5]. The use of AI-assisted techniques in surgical practices has advantages such as reduced postoperative complications, shorter hospital stays, and improved patient prognoses [6], [7].

The videos captured by the camera during minimally invasive surgery serve as the main input for minimally invasive surgery, providing critical information for better decision-making and better care [8]. Traditionally, enabling machines to understand the content of these image sequences and provide assistance to surgeons during or after surgical procedures requires a high quality and quantity of image labeling and supervised learning methods to train. In supervised learning, the precision of the predictions correlates with the number of labeled data based on Hoeffding’s inequality and the union bound [9]. In contrast, humans learn new visual concepts with far fewer labeled examples, in a manner that is akin to self-supervised learning approaches, which rely significantly on the input data examples and only leverage a smaller number of labels in the final training stages for specific tasks. Such approaches are important in the medical domain, especially when we aim to extend surgical AI to new and uncharted surgical procedures, where labeled datasets are often unavailable, highly imbalanced, or restricted due to privacy concerns and infrastructure limitations [8], [10], [11]. In addition to the issues related to limited high quality and quantity of training data in surgery, the taxonomies used in surgical and medical datasets are often narrower compared to the breadth of labels captured in large computer vision datasets [12].

Surgical images and videos, as well as other medical images, are rich in information, containing abundant local features critical to downstream tasks [13]–[15], which makes it even more important for the balance of global and local information with compact representations. For instance, distinguishing between organs such as the liver and the heart often requires not only local information, such as textures and colors, but also global information, such as shapes, similar to how one distinguishes a bird from a dog in ImageNet. Textures and local features are particularly crucial in medical images, especially for diagnostic tasks. For example, detecting fine microcalcifications and details is critical for identifying breast cancers [16]. Similarly, the polyps in the colon vary,

¹Surgical Artificial Intelligence Laboratory, Massachusetts General Hospital, MA, USA. lyin5@mgh.harvard.edu

²Computer Science and Artificial Intelligence Laboratory, Massachusetts Institute of Technology, MA, USA. lianhao,rus@csail.mit.edu

⁴Department of Surgery, Duke University, NC, USA. guy.rosman,ozanan.meireles@duke.edu

Acknowledgement: The authors receive partial research support from the Department of Surgery at Massachusetts General Hospital as well as CRICO

L.Y is the first author. Authors sequence in alphabetical order

and micropolyps are identifiable only with changes in local texture, color, or shape. In summary, surgical image analysis is based on fine-grained phenomena [15], we are still missing self-supervised approaches that can handle such perceptually detailed data while leveraging the limited number of concepts that are used to reason about each section of the video.

We propose a self-supervised learning method that uses Kolmogorov complexity and entropy maximization methods to optimally compress information from local and global views with compact representations, encompassing both semantic and perceptual information and to overcome the bias introduced in the self-supervised training process, such as the Masked Auto Encoder (MAE) [17], to achieve balanced performance across different sets of downstream tasks. The majority of current computer vision approaches in surgery use visual feature backbones that were pre-trained from general images, which is bias from the surgical images. Some works have used the standard MAE method to train with videos of general surgery and demonstrated results in limited tasks such as phase classification [18] and segmentation and limited surgeries such as laparoscopic cholecystectomy [19]. We pre-train the foundation model using the largest surgical image datasets combining both public and private available datasets from Massachusetts General Hospital (MGH) using the proposed self-supervised learning method. The results demonstrate promising outcomes and generalization capability across various downstream tasks using a pre-trained neural network. Downstream tasks can include surgical workflow classification, surgical action classification, segmentation, and diagnosis (Fig. 2), which will be detailed in Section III. We show that the resulting latent compressed visual model, Compress-to-Explore (C2E), provides an effective visual foundation model for surgical video analysis, while catering to both local (perceptual) and global (semantic) aspects of the images [20]. The contributions of the paper are as follows.

- We devise the latent compression transformer architecture and define how to train it to obtain latent compressed representation within the auto-encoder architecture.
- We demonstrated the generalization capability of the proposed self-supervised learning foundation model in various downstream task, compact representation, and few-shot learning capabilities.
- We demonstrate how the approach allows us to expand on a novel dataset with 0.78M images based on 2122 surgeries (845 surgeries collected over 8 years from Massachusetts General Hospital and other 1277 surgeries from open datasets), demonstrating how the approach enables the scaling up of surgical foundation model.

A. Related work

1) *Self-supervised foundation models*: Self-supervised foundation models [21] have been changing multiple domains of AI and many aspects of society. Foundation models are pre-trained using self-supervised method and finetuned in various of downstream tasks. Two main branches of self-supervised learning have been widely researched in computer vision: invariance-based methods and generative methods.

Invariance-based One of the examples of invariance-based methods is contrastive-based learning such as Simple Siamese (SimSiam) [22], [23]. It backpropagates the error through the image encoder by maximizing the similarity of two images augmented from the same image. Some contrastive learning has been applied for pretraining in surgical video analysis [24]–[27]. Another example is the Joint Embedding Predictive Architecture (JEPA) [28], which predicts the embedding of one part of the image using the embedding of the other parts of the same image. Invariance-based self-supervised learning requires balancing the learning of local and global features to optimize performance across downstream tasks, such as classification and segmentation, where, the classification task requires more global features than local features compared to the segmentation task [29]. To address this challenge, several approaches have been proposed, such as using teacher-student networks to capture local and global features [14].

Generative model The widely used generative methods in surgical video analysis are the variational auto encoder (VAE), the masked auto encoder (MAE) [17], the diffusion models [30], etc. The MAE pre-trained encoders were used in various downstream tasks by predicting masked images patches using unmasked images patches, which has shown promise in generalization [19] and will be adopted in this paper. Diffusion-based models are often incorporated in more specific tasks such as segmentation. Such diffusion models have also been used to address the imbalance of training data by generating synthetic images for underrepresented scenarios [31].

2) *Information-based approaches*: Information-based approaches have been used in computer vision [32] and deep neural network design [33]–[35]. Recent works have broadly looked at effective but compact representations [36]–[39]. For example, total coding rate maximization has been used as covariance regularization techniques to avoid collapse of representation, and coding rate reduction inspired design has improved the representation of self-supervised learning [40], [41], segment images [42] and design neural network [35]. The compression of neural network input using the discrete cosine transform (DCT), which is an image compilation method, was shown to be 5 times faster in video language action training and improved evaluation score [43]. This paper proposed a new of information compression leverage Kolmogorov complexity minimization to be explained in Section. II-B.

3) *Energy-based approaches*: Compositionality enables better generalization [44] capacity of neural networks. Several attempts are made to add an energy-based model to the generative model framework work [45] to enable compositional understanding of the scene [46] and better generalization [47]. We adapted the closed-formed model of entropy maximization which represents a general energy-based model formation, and used Langevin sampling of such closed-formed entropy maximization in the decoder design to provide a better compositional and generalizable capability, which will be explained in Section. II-C.

4) *Surgical Computer Vision - Overview and Self-Supervised Learning*: Finally we demonstrate our results in the domain of surgical computer vision. Surgical computer vision has

been extending what AI can understand and act on in the surgical context [48], with a variety of efforts aimed at segmentation [49]–[52], detection [53]–[56], tracking [57], [58], workflow estimation [59], and prediction [60]–[62]. As we pointed out in the introduction, while much of the part work in the field depended on supervised learning or the existence of large labeled datasets, visual foundation models [13], [14], [19], [63] are changing the fields by enabling both superior results as well as forays into new procedures and taxonomies.

II. METHODS

We describe our self-supervised model and training approach in this section. The neural network adopted the MAE structure to use an unmasked part of the image to predict the masked part of the images, using an auto-encoder structure (see Fig. 1). The masking rule is inherited from the MAE structure. We changed the structure of the encoder and decoder accordingly with a compressor encoder and explorer decoder using proposed compression and entropy maximization approaches that will be explained in Section II-B and Section II-C.

A. Notation

The images represented by $I \in \mathbb{R}^{W_{img} \times H_{img} \times 3}$ are the input training data, where W_{img} is the width and H_{img} is the height of the images. The compression step compresses the input I through n steps and the hidden layer of each step is denoted Z_n . The hidden state of the final compression step is Z_0 , h is the hidden state of the temperature measurement within Z_0 that can represent the temperature level of the inputs. Kolmogorov complexity and the complexity of the hidden state are denoted by $K(Z)$, and the entropy of that is defined by $H(Z)$. The \hat{Z} represents an estimation of the hidden state in the decoder. The energy function uses E to represent the energy of the hidden state.

B. Compression encoder

We want to compress the input I to the hidden space $Z_0 \in \mathbb{R}^{N,C}$, which is a disentangled and sparse normal distribution, where N is the number of patches and C is the number of elements. Based on [64] (Theorem 8.4.1), entropy of multi-variable normal distribution is

$$h(Z_1, Z_2, \dots, Z_n) = h(N(\mu, \Sigma)) = \frac{1}{2} \ln(2\pi e)^M |\Sigma| \quad (1)$$

And it can be expanded as Eq. 2.

$$H(Z) = \frac{1}{2} \ln |\Sigma| + \frac{M}{2} (1 + \ln 2\pi) \quad (2)$$

where M is the dimensionality of x . The covariance matrix can be approximated by $\Sigma = \frac{1}{m} Z Z^T$, with Z having a mean of zero due to a normalization layer.

We want to compress I to the hidden state Z_0 with a high compression ratio. We formulate this as maximizing the Kolmogorov complexity difference ($K(Z) - K(I)$) for each compression step. Theory 1 has shown that $\mathbb{E} \frac{1}{n} K(Z^n | n) \rightarrow H(Z)$, which means that the Kolmogorov complexity approaches the

entropy defined in 2. Therefore, for the compression process, maximizing the Kolmogorov complexity difference is equal to maximizing the entropy difference of the input and hidden states as in Eq. 3, with the dimensionality constraints in the equation. Theorem 2 indicates that Eq. 3 is concave and the solution is located at the vertices of feasible sets of hidden states.

$$\begin{aligned} \max_{\theta} & -H(Z) + H(I) \\ & \propto -\frac{1}{2} (\ln |\Sigma_Z| - \ln |\Sigma_I|) + \frac{1}{2} (\Delta M) \\ & \propto -\frac{1}{2} (\ln |\Sigma_Z|) + \frac{1}{2} (\Delta M) \end{aligned} \quad (3)$$

If we assume that the dimension changes are constant, $\frac{1}{2} \Delta M$ will have no influence on the optimization. We also prove that the optimization (Eq. 3) holds with the hidden state with reduced dimension in Theorem 4. In neural network design, before each encoder block project, we remove a constant dimension to enforce the dimension reduction (Fig. 1).

We then use iterative shrinkage-thresholding algorithms to solve the optimization (Eq. 3) in an iterative way, where the step index $i \in [0, n-1]$. Taking $Z = SVD$, the optimization in Eq. 3 can be split into multiple compression steps to compress Z_n to Z_0 in Eq. 4, which minimize the Kolmogorov complexity proved by Theorem. 3.

$$\begin{aligned} Z_{i+\frac{1}{2}} &= Z_{i+1} + \beta \nabla_Z (-H(Z_{i+1})) \\ &= Z_{i+1} - \beta Z_{i+1} (Z_{i+1}^T Z_{i+1})^{-1} \\ &= Z_{i+1} - \beta (S_{i+1} V_{i+1} D_{i+1}) \\ & \quad (D_{i+1}^T V_{i+1} S_{i+1}^T S_{i+1} V_{i+1} D_{i+1})^{-1} \\ &= Z_{i+1} - \beta (S_{i+1} V_{i+1}^{-1} D_{i+1}) \end{aligned} \quad (4)$$

In the end, we applied the linear feedforward layer to project $Z_{i+\frac{1}{2}}$ to subspaces Z_i at each iteration in Eq. 5 with a bypass term. The bypass term is to enable information and gradient propagation through multiple layers of deep neural network as residual function used by ResNet [65].

$$Z_i = Z_{i+\frac{1}{2}} + P Z_{i+\frac{1}{2}} \quad (5)$$

Based on Theorem 5, mapping $Z_{i+\frac{1}{2}}$ to subspaces where $P^T P = \Pi$ maximize the compression, where, $\Pi \in \mathbb{R}^{C,C}$ is a diagonal matrix with $\pi_i \in [0, 1]$. The decoder used inverse of such mapping. We note that in our implementation, we use S, V, D, P , conditioned on the input to each layer, as linear operators, without constraining them into their specific matrix manifold [66].

C. Exploration decoder

The motivation of an exploration decoder is that an inverse compression process is to maximize entropy to reconstruct the images. The solutions of entropy maximization in a closed-form solution are in energy functions formulation, whereas the energy-based neural network in the decoder design has the potential to have a better capability of generalization. The other motivation is that the entropy maximization process itself can also improve the representation and compression process.

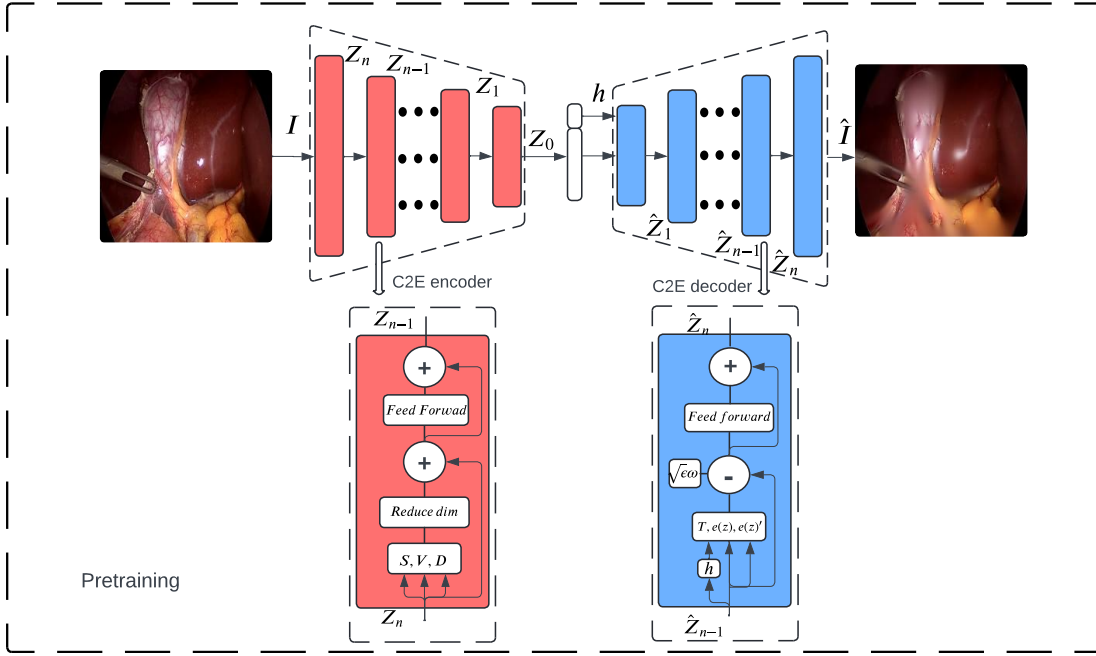


Fig. 1. C2E General structure. In pretraining, the encoder compresses the raw images patches I into hidden state Z_0 using n layers of proposed encoder structure. The output of hidden state of each layer is named as Z_i , where $i \in [0, n]$. The decoder reconstructs the images patches and the output of each layer are as estimate of hidden state \hat{Z}_i , where $i \in [0, n]$. The error of the reconstructed images and the raw images are backpropagated to the neural network during the training process. In pretrained encoder were used to extract features from the videos and used for a few downstream tasks (Fig. 2) such as surgical work flow prediction, surgeons' action prediction, segmentation, diagnosis.

From the maximization of entropy with the expectation of an energy function $E(z)$ as a neural network, where z is the sample of elements of Z , the probability of state at the energy of $E(z)$ is p_k which is the solution of maximization of Eq. 6 [67] with Lagrange multipliers.

$$J = -K \sum_{k=1}^n p_k \log(p_k) + \lambda(1 - \sum_{i=1}^n p_k) + \mu(\mathbb{E}[E(z)] - \sum_{k=1}^n p_k E(z_k)) \quad (6)$$

The probability of the state of an individual particle is a function of the expectation of function $E(z)$. Taking $E(z)$ as energy, we can get Eq. 7 as a closed-form solution of Eq. 6.

$$p(z) \propto e^{-\frac{1}{\mathbb{E}[E(z)]} E(z)} \quad (7)$$

The samples of z are conditioned on the expectation of energy $\mathbb{E}[E(z)]$ that is proportional to the temperature $kT(h)$, where the temperature can be represented as a function of a hidden state h .

$$\mathbb{E}[E(z)] = kT(h) \quad (8)$$

With Langevin dynamics, the hidden state can be sampled by following steps:

$$\hat{Z}_i = \hat{Z}_{i-1} + \epsilon \nabla \log p(\hat{Z}_i) + \sqrt{2\epsilon\omega_i} \omega_i \sim N(0, I) \quad (9)$$

where N is a multivariate Gaussian, and $i \in [0, n]$.

Plug in Eq. 7 to Eq. 9, and combine an inverse process of Eq. 5, we can estimate the hidden state in iterative way

Eq. 10, 11, which is also illustrated in Fig. 1.

$$\hat{Z}_{k-\frac{1}{2}} = \hat{Z}_{k-1} - \epsilon \frac{1}{kT(h)} E(\hat{Z}_{k-1}) E(\hat{Z}_{k-1})' + \sqrt{2\epsilon\omega_i} \omega_i \quad (10)$$

$$\hat{Z}_i = \hat{Z}_{i-\frac{1}{2}} + P^{-1} \hat{Z}_{i-\frac{1}{2}} \quad (11)$$

Since the data are limited and the samples in each subspace of Z_0 are normally distributed, the temperature can be estimated by part of the subspace within which the hidden states are uniformly distributed. The temperature of the exploration samples is conditioned by partial elements of Z_0 , which is proved by Theorem 6. In the implementation, we proposed a conditional ratio $\beta \in [0, 1]$ to enforce partial elements of hidden states to represent the total hidden states.

$$h = E_c(Z_0, \beta) \quad (12)$$

D. Pre-training

For pretraining, we used videos from various open source surgical videos including laparoscopic cholecystectomy, proctocolectomy, rectal resection, sigmoid resection, gynecologic laparoscopy, radical prostatectomy, sleeve gastrectomy, and the largest surgical video datasets in general surgery from Massachusetts General Hospital. We take 1 fps frame extracted from the raw videos and filtered the images by deduplicating them [68], and then using CLIP-based image quality assessment [69] to keep only distinct and high-quality images, to have a dataset with largest image diversity in surgery.

We also remove the images that were used for downstream tasks to avoid data leakage. The resulting datasets for pretraining include 2122 surgeries and 0.78M images (Tab. I).

As stated in Theorem 1, the objective of the compression process is convex and differentiable. The loss function minimizes the mean average error of the predicted images (\hat{I}) and the original images (I), making the overall training run as a standard MAE [17] pipeline.

TABLE I
PRETRAINING DATASETS

Surgical categories	Surgical datasets	Surgery numbers	Unique images
Lap Chole	Cholec80	80	30000 [70]
	hSDB instrument	24	10000 [71]
Proctocolectomy Rectal Resection	HeiCo	10	14448 [72]
	HeiCo	10	19528
Sigmoid Resection	DSAD	32	4239 [73]
	HeiCo	10	16037
Gynecologic laparoscopy	LapGyn4	500	10000 [74]
	SurgicalActions160	59	491 [75]
	GLEND A	> 400	578 [76]
Radical prostatectomy	ESAD	4	5768 [77]
Sleeve gastrectomy	MGH	86	135766
General surgery	MGH18k	845	531565
Total		2122	788420

III. RESULTS

We proceed to explore the performance of our model. We demonstrate that the proposed method has a strong generalization capacity as a pre-trained encoder in various downstream tasks and in various surgery types, thus functioning as a visual foundation model for surgery. We then proceed to analyze the intermediate representations afforded by the model, which demonstrate its superior ability to disentangle known medical concepts such as different tools, surgical phases, and type of procedure.

For quantitative results on downstream tasks, we examine the model’s few-shot behavior across a variety of procedures and ML tasks in Section III-E. We focus on standard fine-tuning ML tasks in Sections III-A-III-D. For each of the downstream tasks, we connect the pre-trained encoder to downstream-task decoder (Fig. 1) for fine-tuning, demonstrating how the model functions as a surgical foundation model and enables task generalization. To provide a fair comparison, we selected related work using base size of encoder which is similar to our encoder size (85.22M parameters for encoder) to contrast in the results. The pre-trained encoder also demonstrated better few-shot learning capability in out-of-distribution datasets in Section III-E.

For qualitative analysis, to provide more insights of neural network representation, we also analyzed the representation and saliency maps of various tasks in Section III-F.

A. Surgical workflow prediction

Surgery typically progresses through distinct phases during treatment. Automatically understanding and analyzing the surgical workflow can yield valuable insights, such as detecting abnormalities such as unusually prolonged or shortened phase durations or identifying skipped phases. These will provide warning and prediction of the next step for surgeons and therefore improve patient care. Specifically, workflow prediction

can be formulated as a classification problem in the downstream task. We adopted Cholec80 datasets for the evaluation of the workflow prediction of cholecystectomy surgery. The Cholec80 datasets [70] contains 80 cholecystectomy surgery videos, annotated with 7 distinct phase labels. We used the official splitting (40 videos for training and 40 videos for testing). The results show that the proposed method can improve the classification accuracy by replacing the TeCNO backbone in the downstream task (Tab. II).

TABLE II
SOTA IN PHASE RECOGNITION WITH CHOLEC80

Method	Accuracy	Precession
EndoNet [70]	81.7 ± 4.2	73.7 ± 16.1
EndoNet+LSTM [78]	88.6 ± 9.6	84.4 ± 7.9
MTRCNet-CL [79]	89.2 ± 7.6	86.9 ± 4.3
PhaseNet [70], [80]	78.8 ± 4.7	71.3 ± 15.6
SV-RCNet [81]	85.3 ± 7.3	80.7 ± 7.0
TeCNO [82]	88.6 ± 7.8	86.5 ± 7.0
Trans-SVNet [83]	90.3 ± 7.1	90.7 ± 5.0
LoViT [84]	91.5 ± 6.1	83.1 ± 9.3
SurgFormer [85]	92.4 ± 6.4	87.9 ± 6.9
C2E(ours)	92.5 ± 6.9	83.2 ± 13.9

B. Surgeon’s action

Monitoring and forecasting surgeons’ actions in real time provides detailed information on what tissues and what tools the surgeon is working on. This monitoring and forecasting will prevent problems such as surgeon cutting or resecting in wrong-target tissues or in the wrong phase of a surgery. In the end, this improves the safety and patient care. We used the evaluation metrics proposed for the CholecT45 [86] data set for the downstream task. We adopted Rendezvous method using focal loss and long videos as input without changing the decoder structure and only changing the backbones. The proposed method has better average precision in detecting taken, tissues, tool-tissue interaction, tool-action pair, and action-tool-tissue pairs (tab. III).

TABLE III
COMPARISON OF THE PROPOSED METHOD WITH RELATED WORK IN ACTION TRIPLET

Method	mAP_{it}	mAP_{iv}	mAP_{iwt}
Tripnet [87]	27.1 ± 2.8	31.8 ± 4.1	24.4 ± 4.7
Attention Triplet [88]	29.4 ± 1.2	33.0 ± 2.9	27.2 ± 2.7
Rendezvous [88]	30.8 ± 2.1	34.0 ± 3.3	29.4 ± 2.8
ConceptNet-ViT [89]	33.4 ± 3.2	33.7 ± 3.2	30.6 ± 1.9
RiT [90]	36.9 ± 1.0	38.3 ± 3.5	29.7 ± 2.6
MT4MTL(No Ensemble) [13]	43.1 ± 2.0	44.9 ± 2.4	37.1 ± 0.5
LAM [91]	-	-	35.9
ours	42.3 ± 0.9	48.6 ± 2.1	41.8 ± 0.9

C. Segmentations in surgery images

Identifying distinguished anatomical structures is critical during surgery. A high accuracy of such task will improve the performance of the correct dissection, resection, and cutting. To have a fair comparison, we compared the proposed method with the method using the same fine-tuning structure. The proposed method has shown improved performance (see

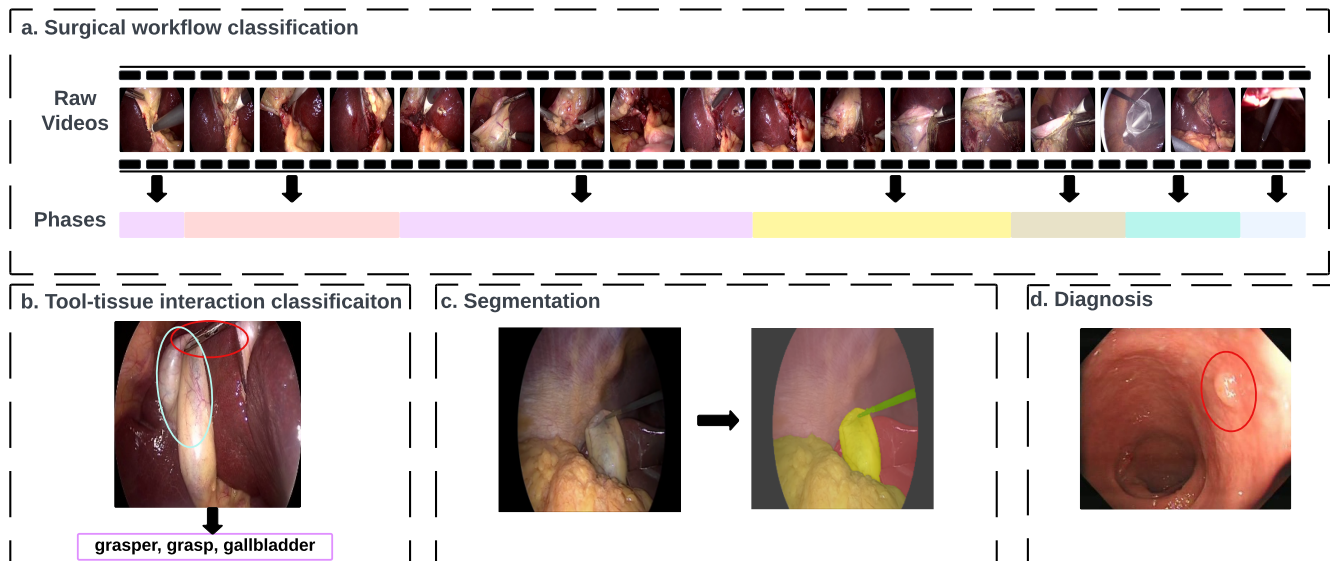


Fig. 2. The generalization of the pretrained encoder was evaluated across various downstream tasks, such as (a) workflow classification, (b) action classification, (c) segmentation, and (d) diagnosis

Tab. IV) using the CholecSeg8k dataset [52], adopting the downstream decoder from the Dense Prediction Transformer (DPT) decoder. A demonstration (Fig. 3) of segmentation of the proposed methods shows a small difference between target and predicted segmentation.

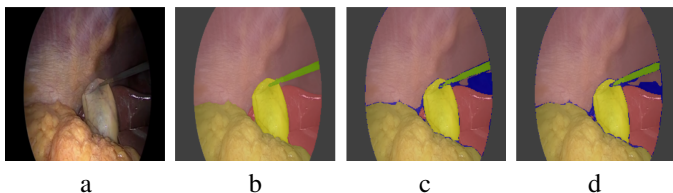


Fig. 3. Comparison of segmentation using VIT and C2E. a: The original input image. b: The ground truth of the segmentation. Subfigure c and d indicate the difference of ground truth of and prediction Segmentation using VIT(c) and C2E(d). The blue parts are the difference. Our proposed method has smaller difference (small blue areas) and has better semantic segmentation on the area between tool, liver and background

TABLE IV

SEGMENTATION APPROACHES COMPARISON ON THE CHOLECSEG8K DATASET

Method	IoU
Adaptive SAM [92]	0.64
MedT [93]	0.57
TransUNet [94]	0.62
DeepLabV3+ [95]	0.56
UNetR [96]	0.55
DynUnet [97]	0.55
U-Net++ [98]	0.62
U-Net [99]	0.48
SAMed [100]	0.41
Low Rank Adaptation of SAM [101]	0.65
S-SAM [102]	0.71
SegDepth [103]	0.556
DDA [104]	0.59
CLU [105]	0.463
C2E (ours)	0.74

D. Intraoperative polyp diagnosis

Detection and diagnosis of microtumor and polyps instruct surgeons and physicians to have early detection of cancer, reduce colorectal cancer mortality, reduce the cost of treatment with the costly treatment required for advanced cancer, and improve patient outcomes. Specifically, detection and diagnosis in colonoscopy can help to take the right decision on if they need to dissect the polyps for further pathology tests in tumors and if they need to resect and dissect polyps attached to the colon. We adopted the PolypDiag data set [106] for evaluation. For the fine-tuning settings, we used linear layer as decoder. The results have shown improvement in this task compared to several related works.

TABLE V

APPROACH COMPARISON ON POLYP DIAGNOSIS

Method	Accuracy[%]
ProViCo[26] [107]	86.9±0.5
VCL [108]	87.6±0.6
ST-Adapter [109]	84.8±0.7
EndoSSL [23]	91.3±0.6
EndoFM [14]	90.7±0.4
C2E (ours)	94.0±0.7

E. Few-shot Analysis

Several questions arise when comparing our approach to other self-supervised visual foundation models. We give an example of the proposed method by comparing it to a VIT model [110], such as the one used in [19], showing improved performance using the same datasets (see Tab. I) for our dataset content, significantly expanding on [19]). We compare the models in a variety of downstream tasks – those of phase recognition, action prediction, and segmentation, and obtain superior results, as shown in Tab. VI).

We note that the ability to facilitate few-shot learning is important, especially when we wish to extend surgical

TABLE VI
ABLATION OF MODEL WITH DATASETS IN LAPAROSCOPY
CHOLECYSTECTOMY

model	Acc(ele)	mAP_{ivt}	IOU	Acc
	Phase	Action triplet	Segmentation	Diagnosis
VIT	89.7 ± 0.5	40.3 ± 2.2	73.5 ± 0.3	92.5 ± 2.2
C2E(ours)	92.5 ± 6.9	41.8 ± 0.9	74.2 ± 0.3	94.0 ± 0.7

AI to novel procedures, which may not have many labeled procedures and yet possess a great potential to improve patient care and surgical results, such as [111]. As an additional test for the foundation model property, we test explicitly the few-shot generalization of the proposed approach. We adapted HeiCo datasets for phase classification in a few-shot setting, including proctocolectomy (10 videos), rectal resection (10 videos), and sigmoid resection (10 videos). Our approach enables better few-shot capability at the limit of few procedures, as shown in Tab. VII, VIII.

TABLE VII

COMPARISON OF FEW-SHOT PHASE RECOGNITION, 8 VIDEOS.

Proc.	Lap. Chole.	Proctoc- olectomy	Rectal resect.	Sigmoid resect.
Method	8 vid.	8 vid.	8 vid.	8 vid.
VIT	75.84 ± 2.76	$58.8 \pm 11.$	60.2 ± 0.1	60.2 ± 0.1
C2E	85.7 ± 0.37	84.6 ± 2.2	79.3 ± 8.7	76.2 ± 5.3

TABLE VIII

COMPARISON OF FEW-SHOT PHASE RECOGNITION, 2 VIDEOS.

Proc.	Lap. Chole.	Proctoc- olectomy	Rectal resect.	Sigmoid resect.
Method	2 vid.	2 vid.	2 vid.	2 vid.
VIT	67.16 ± 3.00	44.06 ± 0.19	58.57 ± 3.80	58.57 ± 3.80
C2E	78.21 ± 3.90	61.24 ± 0.13	67.34 ± 0.01	64.33 ± 5.92

F. Representation Insights

To examine what representations are learned by the model and how well they capture and disentangle relevant surgical factors, compared to standard visual models, we visualize the two-dimensional t-SNE figure using various classes such as different types of surgery (Fig. 4), phases of laparoscopic cholecystectomy (Fig. 5), and instruments of laparoscopic cholecystectomy (Fig. 6). The features of the proposed methods are more separated compared to those obtained by probing the features obtained from [19]. This explains why it shows promise in the few-shot learning and capability of generalization.

We visualize the saliency maps of Fig. 7 to provide more insights of representation of the neural networks. Compared to VIT based encoder, the saliency maps are more compact. More importantly, the peak of attention of each head differs from each other. This attention distribution demonstrated that each head represents specific local features and details information and the aggregation of multi-heads represents the global information, which creates a better balance of representation of local and global information.

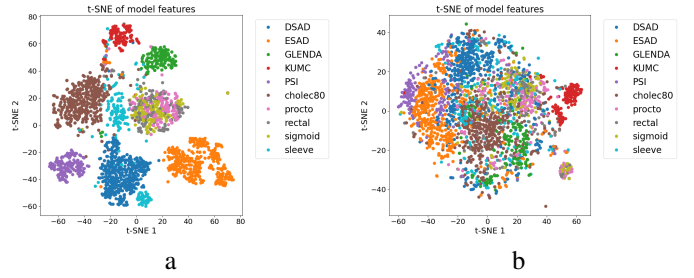


Fig. 4. T-SNE feature visualization of our C2E approach (a) vs MAE (b) for frames from a variety of procedures. Notice how each procedure is mapped to a different cluster in the embedded space, in a more pronounced way, compared to the entangled clusters in MAE.

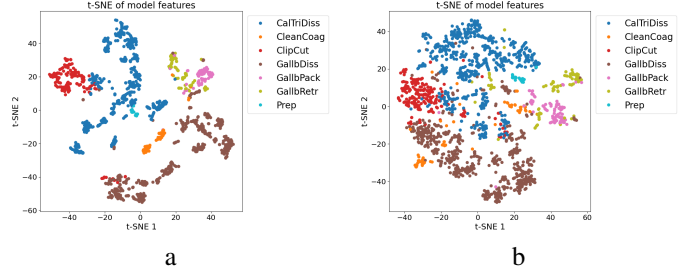


Fig. 5. T-SNE feature visualization of our C2E approach (a) vs MAE (b), for phases from Laparoscopic Cholecystectomy procedures. Each phase is mapped to a more separated clustered group in the embedded space compared to the entangled clusters in MAE.

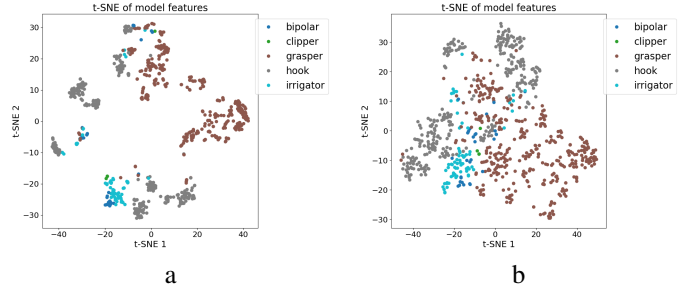


Fig. 6. T-SNE feature visualization of our C2E approach (a) vs MAE (b), for frames from Laparoscopic Cholecystectomy procedures. The embeddings of different instruments are disentangled in reduced dimensions.

IV. CONCLUSION

In conclusion, we leverage the compression method and entropy maximization to encourage the compression of images and improve the representation of neural network in pertaining. The pre-trained backbone has shown promising performances in various downstream tasks in the surgical artificial intelligence domain, such as workflow prediction, robotic action, segmentation, and diagnosis. We envision that the proposed self-supervised learned foundation model can reduce the labeling quantities required for various downstream tasks since high-quality annotation in surgical videos is limited due to privacy and high working load. It will enable an improved quality of various monitoring tasks and reduce the complication of surgery, and improve quality of treatment.

V. MAIN THEORETICAL CONTRIBUTION

Theorem 1: The entropy of the image embeddings $H(X)$ is the Kolmogorov complexity $K(X)$ of image embeddings in

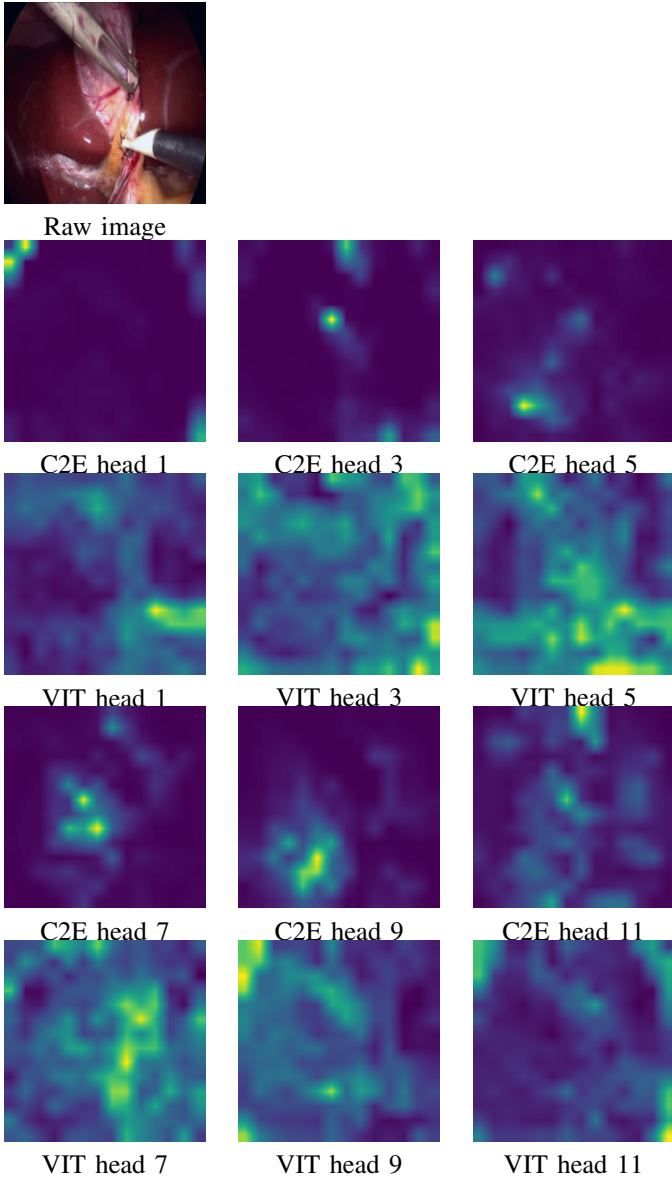


Fig. 7. Saliency map comparison of C2E and ViT head. The proposed method C2E has a relative sparsity of the activation maps indicating a more compressed representation. The high attention region of each heads with C2E are complementary and not overlapped indicating that the information of images are decomposed into different local information in each heads and represent global by aggregation.

compression.

Proof: Based on Theorem 14.3.1 [64]

$$H(x) \leq \mathbb{E} \frac{1}{n} K(X) \leq H(X) + \frac{(|\chi| - 1) \log n + c}{n} \quad (13)$$

$$\mathbb{E} \frac{1}{n} K(X) \rightarrow H(X) \quad (14)$$

This equation holds on condition of $x \in \chi$ is finite. The domain of input information of the images is finite. The transformation of input to the hidden state is also finite.

Therefore, the Kolmogorov complexity $K(X)$ approaches the entropy $H(x)$ for large n . ■

Theorem 2: The compression function Eq. 3 is convex

Proof: Combine Eq. 2 and Eq. 3

$$\begin{aligned} & -H(Z_{i+1}) + H(I_{i+1}) \\ &= -\frac{1}{2} \ln |\Sigma| - \frac{D}{2} (1 + \ln 2\pi) + H(I_{i+1}) \end{aligned} \quad (15)$$

Based on Theorem 7.6.7 in [112] the function $\ln |A|$ is a strictly concave function on the convex set of positive definite Hermitian matrices.

While Σ is positive definite Hermitian, therefore, $\ln |\Sigma|$ is concave.

The $-\frac{1}{2} \ln |\Sigma|$ is convex. The solution of maximization is located on the edges of the scope of hidden space. ■

Theorem 3: The gradient step Eq. 4 minimizes Kolmogorov complexity.

Proof: Consider constant n during training. Equation 4 minimizes $H(Z)$ which is a higher bound of $K(X)$. Therefore, optimization minimizes Kolmogorov complexity. ■

Theorem 4: The stepwise dimension reduction process in Eq. 1 is equivalent to maximizing the compression step in Eq. 3.

Proof:

$$\begin{aligned} & (H(Z_i) - H(Z_{i+\frac{1}{2}})) \\ &= \frac{1}{2} (\ln |Z_i| - \ln |Z_{i+1}| - |z_i| \nabla_{Z_{i+1}} (\ln |Z_{i+1}|)) \quad (16) \\ &= \frac{1}{2} (\ln |Z_i| - \ln |Z_{i+1}| - |z_i| |Z_{i+1}|^{-1}) \end{aligned}$$

where, $Z_{i+\frac{1}{2}}$ is the hidden state without dimension reduction. From first to second equation use Taylor expansion and the $|Z_i| \gg |z_{i+1}|$ and the dimensionality of $\dim(z_i) \ll \dim(Z_{i+1})$, therefore the following equation holds

$$\begin{aligned} & \arg \max_{Z_{i+\frac{1}{2}}} H(Z_i) - H(Z_{i+\frac{1}{2}}) \\ &= \arg \max_{Z_{i+1}} \frac{1}{2} (\ln |Z_i| - \ln |Z_{i+1}|) \end{aligned} \quad (17)$$

■
Theorem 5: The mapping of embedding Z to an orthogonal subspace maximizes the Kolmogorov complexity difference defined as $-H(Z) + H(I)$

Proof: Since $\ln |Z|$ is concave, Z is a positive definite Hermitian matrix.

$$\max_Z \frac{1}{2} (-\ln |Z|) = \min_Z \ln (|Z|) \quad (18)$$

since $\ln(Z^T \Pi_i Z)$ has a lower bound of $\sum_i^k \ln(Z^T \Pi_i Z)$ where, $\Pi \in R^{C,C}$ is a diagonal matrix with $\pi_i \in [0, 1]$ and $\sum_i^k \Pi_i$ as identity matrix.

$$\begin{aligned} & \max_Z \frac{1}{2} (-\ln |Z|) = \min_Z \ln (|Z|) \\ &= \min_{Z, \Pi} \sum_i^k \ln(Z^T \Pi_i Z) \end{aligned} \quad (19)$$

As $\ln(Z^T \Pi_i Z)$ is a concave function (Theorem 7.6.7 in [112]) for $Z^T \Pi_i Z$ to be positive semi-defined. The global minimization is at the boundary of the convex domain, where $\pi_i \in \{0, 1\}$. This shows that Π_i maps Z to the k subspace to maximize the compression.

Theorem 6: The temperature T defined in expectation of energy $\mathbb{E}[e(z)] = kT$ in Eq. 10 is conditioned by partial elements of the hidden state z

Assumption 1: The distribution of particles z in all its subspaces is homogeneous.

Proof: The z can be split into two groups $z = [z_{sub_i}, z_{sub_j}]$. Per Assumption 1,

$$\mathbb{E}[e(z)] = \mathbb{E}[e(z_{sub_i})] \quad (20)$$

REFERENCES

- [1] N. Oh, J.-H. Kim, J. Rhu, W. K. Jeong, G.-s. Choi, J. M. Kim, and J.-W. Joh, "Automated 3d liver segmentation from hepatobiliary phase mri for enhanced preoperative planning," *Scientific Reports*, vol. 13, no. 1, p. 17605, 2023.
- [2] X. Chen, H. Xu, Q. Qi, C. Sun, J. Jin, H. Zhao, X. Wang, W. Weng, S. Wang, X. Sui, et al., "Ai-based chest ct semantic segmentation algorithm enables semi-automated lung cancer surgery planning by recognizing anatomical variants of pulmonary vessels," *Frontiers in Oncology*, vol. 12, p. 1021084, 2022.
- [3] N. Haouchine, J. Dequidt, I. Peterlík, E. Kerrien, M. Berger, and S. Cotin, "Image-guided simulation of heterogeneous tissue deformation for augmented reality during hepatic surgery," 2013.
- [4] P. Mascagni, D. Alapatt, L. Sestini, M. S. Altieri, A. Madani, Y. Watanabe, A. Alseidi, J. A. Redan, S. Alfieri, G. Costamagna, et al., "Computer vision in surgery: from potential to clinical value," *npj Digital Medicine*, vol. 5, no. 1, p. 163, 2022.
- [5] J. Zhang, S. Zhou, Y. Wang, S. Shi, C. Wan, H. Zhao, X. Cai, and H. Ding, "Laparoscopic image-based critical action recognition and anticipation with explainable features," *IEEE J. Biomed. Health Inform.*, vol. 27, pp. 5393–5404, Nov. 2023.
- [6] M. X. Morris, D. Fiocco, T. Caneva, P. Yiapanis, and D. P. Orgill, "Current and future applications of artificial intelligence in surgery: implications for clinical practice and research," *Front. Surg.*, vol. 11, p. 1393898, May 2024.
- [7] H. Ashrafi, "Artificial intelligence in surgery: the future is now," *Eur Surg Res*, vol. 65, pp. 22–39, 2024.
- [8] M. F. Avram, D. C. Lazăr, M. I. Mariş, and S. Olariu, "Artificial intelligence in improving the outcome of surgical treatment in colorectal cancer," *Front. Oncol.*, vol. 13, p. 1116761, Jan. 2023.
- [9] S. Shalev-Shwartz and S. Ben-David, *Understanding machine learning: From theory to algorithms*. Cambridge university press, 2014.
- [10] O. R. Meireles, G. Rosman, M. S. Altieri, L. Carin, G. Hager, A. Madani, N. Padoy, C. M. Pugh, P. Sylla, T. M. Ward, D. A. Hashimoto, and SAGES Video Annotation for AI Working Groups, "SAGES consensus recommendations on an annotation framework for surgical video," *Surg. Endosc.*, vol. 35, pp. 4918–4929, Sept. 2021.
- [11] J. A. Eckhoff, G. Rosman, M. S. Altieri, S. Speidel, D. Stoyanov, M. Anvari, L. Meier-Hein, K. März, P. Jannin, C. Pugh, M. Wagner, E. Witkowski, P. Shaw, A. Madani, Y. Ban, T. Ward, F. Filicori, N. Padoy, M. Talamini, and O. R. Meireles, "SAGES consensus recommendations on surgical video data use, structure, and exploration (for research in artificial intelligence, clinical quality improvement, and surgical education)," *Surg. Endosc.*, vol. 37, pp. 8690–8707, Nov. 2023.
- [12] J. Deng, A. C. Berg, K. Li, and L. Fei-Fei, "What does classifying more than 10,000 image categories tell us?," in *Computer Vision—ECCV 2010: 11th European Conference on Computer Vision, Heraklion, Crete, Greece, September 5–11, 2010, Proceedings, Part V 11*, pp. 71–84, Springer, 2010.
- [13] S. Gui, Z. Wang, J. Chen, X. Zhou, C. Zhang, and Y. Cao, "MT4MTL-KD: A multi-teacher knowledge distillation framework for triplet recognition," *IEEE Trans. Med. Imaging*, vol. 43, pp. 1628–1639, Apr. 2024.
- [14] Z. Wang, C. Liu, S. Zhang, and Q. Dou, "Foundation model for endoscopy video analysis via large-scale self-supervised pre-train," in *Medical Image Computing and Computer Assisted Intervention – MICCAI 2023*, pp. 101–111, Springer Nature Switzerland, 2023.
- [15] C. F. Sabottke and B. M. Spieler, "The effect of image resolution on deep learning in radiography," *Radiol. Artif. Intell.*, vol. 2, p. e190015, Jan. 2020.
- [16] K. Rangarajan, A. Gupta, S. Dasgupta, U. Marri, A. K. Gupta, S. Hari, S. Banerjee, and C. Arora, "Ultra-high resolution, multi-scale, context-aware approach for detection of small cancers on mammography," *Sci. Rep.*, vol. 12, p. 11622, July 2022.
- [17] K. He, X. Chen, S. Xie, Y. Li, P. Dollár, and R. Girshick, "Masked autoencoders are scalable vision learners," in *Proceedings of the IEEE/CVF conference on computer vision and pattern recognition*, pp. 16000–16009, 2022.
- [18] T. J. Jaspers, R. L. de Jong, Y. Al Khalil, T. Zeelenberg, C. H. Kusters, Y. Li, R. C. van Jaarsveld, F. H. Bakker, J. P. Ruurda, W. M. Brinkman, et al., "Exploring the effect of dataset diversity in self-supervised learning for surgical computer vision," in *MICCAI Workshop on Data Engineering in Medical Imaging*, pp. 43–53, Springer, 2024.
- [19] D. Batić, F. Holm, E. Özsoy, T. Czempiel, and N. Navab, "Endovit: pretraining vision transformers on a large collection of endoscopic images," *International Journal of Computer Assisted Radiology and Surgery*, vol. 19, no. 6, pp. 1085–1091, 2024.
- [20] R. Rombach, A. Blattmann, D. Lorenz, and others, "High-resolution image synthesis with latent diffusion models," *Proceedings of the*, 2022.
- [21] R. Bommasani, D. A. Hudson, E. Adeli, R. Altman, S. Arora, S. von Arx, M. S. Bernstein, J. Bohg, A. Bosselut, E. Brunskill, et al., "On the opportunities and risks of foundation models," *arXiv preprint arXiv:2108.07258*, 2021.
- [22] X. Chen and K. He, "Exploring simple siamese representation learning," *arXiv [cs.CV]*, pp. 15750–15758, Nov. 2020.
- [23] R. Hirsch, M. Caron, R. Cohen, A. Livne, R. Shapiro, T. Golany, R. Goldenberg, D. Freedman, and E. Rivlin, "Self-supervised learning for endoscopic video analysis," *arXiv [cs.CV]*, Aug. 2023.
- [24] Y. Yu, Z. Zhao, Y. Jin, G. Chen, Q. Dou, and P.-A. Heng, "Pseudo-label guided cross-video pixel contrast for robotic surgical scene segmentation with limited annotations," in *2022 IEEE/RSJ International Conference on Intelligent Robots and Systems (IROS)*, pp. 10857–10864, IEEE, Oct. 2022.
- [25] G. Yengera, D. Mutter, J. Marescaux, and N. Padoy, "Less is more: Surgical phase recognition with less annotations through self-supervised pre-training of cnn-lstm networks," *arXiv preprint arXiv:1805.08569*, 2018.
- [26] D. Neimark, O. Bar, M. Zohar, G. D. Hager, and D. Asselmann, "train one, classify one, teach one"–cross-surgery transfer learning for surgical step recognition," in *Medical Imaging with Deep Learning*, pp. 532–544, PMLR, 2021.
- [27] S. Ramesh, V. Srivastav, D. Alapatt, T. Yu, A. Murali, L. Sestini, C. I. Nwoye, I. Hamoud, S. Sharma, A. Fleurentin, et al., "Dissecting self-supervised learning methods for surgical computer vision," *Medical Image Analysis*, vol. 88, p. 102844, 2023.
- [28] M. Assran, Q. Duval, I. Misra, P. Bojanowski, P. Vincent, M. Rabbat, Y. LeCun, and N. Ballas, "Self-supervised learning from images with a joint-embedding predictive architecture," *arXiv [cs.CV]*, pp. 15619–15629, Jan. 2023.
- [29] A. Bardes, J. Ponce, and Y. LeCun, "VICRegL: Self-supervised learning of local visual features," in *Advances in Neural Information Processing Systems* (S. Koyejo, S. Mohamed, A. Agarwal, D. Belgrave, K. Cho, and A. Oh, eds.), vol. 35, pp. 8799–8810, Curran Associates, Inc., 2022.
- [30] J. Ho, A. Jain, and P. Abbeel, "Denoising diffusion probabilistic models," *arXiv [cs.LG]*, pp. 6840–6851, June 2020.
- [31] A. Kazerouni, E. K. Aghdam, M. Heidari, R. Azad, M. Fayyaz, I. Hacıhaliloğlu, and D. Merhof, "Diffusion models for medical image analysis: A comprehensive survey," *arXiv [eess.IV]*, Nov. 2022.
- [32] A. K. Jain, "A fast karhunen-loeve transform for a class of random processes," *IEEE Transactions on Communications*, vol. 24, no. 9, pp. 1023–1029, 1976.
- [33] Y. Ma, H. Derksen, W. Hong, and J. Wright, "Segmentation of multivariate mixed data via lossy data coding and compression," *IEEE transactions on pattern analysis and machine intelligence*, vol. 29, no. 9, pp. 1546–1562, 2007.
- [34] S. Arora, A. Bhaskara, R. Ge, and T. Ma, "Provable bounds for learning some deep representations," in *International conference on machine learning*, pp. 584–592, PMLR, 2014.
- [35] Y. Yu, S. Buchanan, D. Pai, T. Chu, Z. Wu, S. Tong, B. Haeffele, and Y. Ma, "White-box transformers via sparse rate reduction," *Advances in Neural Information Processing Systems*, vol. 36, pp. 9422–9457, 2023.
- [36] N. Tishby and N. Zaslavsky, "Deep learning and the information bottleneck principle," in *2015 IEEE information theory workshop (itw)*, pp. 1–5, Ieee, 2015.

- [37] A. Elad, D. Haviv, Y. Blau, and T. Michaeli, "Direct validation of the information bottleneck principle for deep nets," 2019.
- [38] Z. Goldfeld and Y. Polyanskiy, "The information bottleneck problem and its applications in machine learning," 2020.
- [39] Z. Lyu, G. Aminian, and M. Rodrigues, "On neural networks fitting, compression, and generalization behavior via information-bottleneck-like approaches," 2023.
- [40] Z. Li, Y. Chen, Y. LeCun, and F. T. Sommer, "Neural manifold clustering and embedding," *arXiv preprint arXiv:2201.10000*, 2022.
- [41] X. Liu, Z. Wang, Y.-L. Li, and S. Wang, "Self-supervised learning via maximum entropy coding," *Advances in neural information processing systems*, vol. 35, pp. 34091–34105, 2022.
- [42] Y. Ma, H. Derksen, and W. Hong, "Segmentation of multivariate mixed data via lossy data coding and compression," *IEEE Trans. Pattern Anal. Mach. Intell.*, vol. 29, pp. 1546–1562, Sept. 2007.
- [43] K. Pertsch, K. Stachowicz, B. Ichter, D. Driess, S. Nair, Q. Vuong, O. Mees, C. Finn, and S. Levine, "Fast: Efficient action tokenization for vision-language-action models," *arXiv preprint arXiv:2501.09747*, 2025.
- [44] B. M. Lake and M. Baroni, "Human-like systematic generalization through a meta-learning neural network," *Nature*, vol. 623, no. 7985, pp. 115–121, 2023.
- [45] Y. Du, S. Li, Y. Sharma, J. Tenenbaum, and I. Mordatch, "Unsupervised learning of compositional energy concepts," *Advances in Neural Information Processing Systems*, vol. 34, pp. 15608–15620, 2021.
- [46] N. Gkanatsios, A. Jain, Z. Xian, Y. Zhang, C. Atkeson, and K. Fragkiadaki, "Energy-based models are zero-shot planners for compositional scene rearrangement," *arXiv preprint arXiv:2304.14391*, 2023.
- [47] Y. Du, S. Li, and I. Mordatch, "Compositional visual generation with energy based models," *Advances in Neural Information Processing Systems*, vol. 33, pp. 6637–6647, 2020.
- [48] D. A. Hashimoto, G. Rosman, D. Rus, and O. R. Meireles, "Artificial intelligence in surgery: Promises and perils," *Ann. Surg.*, vol. 268, pp. 70–76, July 2018.
- [49] S. Bodenstedt, J. Görtler, M. Wagner, H. Kenngott, B. Müller-Stich, R. Dillmann, and S. Speidel, "Superpixel-based structure classification for laparoscopic surgery," 2016.
- [50] L. C. García-Peraza-Herrera, W. Li, L. Fidon, C. Grujthuijzen, A. Devreker, G. Attilakos, J. Deprest, E. V. Poorten, D. Stoyanov, T. Vercauteren, and S. Ourselin, "ToolNet: Holistically-nested real-time segmentation of robotic surgical tools," in *2017 IEEE/RSJ International Conference on Intelligent Robots and Systems (IROS)*, pp. 5717–5722, IEEE, Sept. 2017.
- [51] M. Allan, S. Kondo, S. Bodenstedt, S. Leger, R. Kadkhodamohammadi, I. Luengo, F. Fuentes-Hurtado, E. Flouty, A. K. Mohammed, M. Pedersen, A. Kori, A. Varghese, G. Krishnamurthi, D. Rauber, R. Mendel, C. Palm, S. Bano, G. Saibro, C. Shih, H. Chiang, J. Zhuang, J. Yang, V. Igloukov, A. Dobrenkii, M. Reddiboina, A. Reddy, X. Liu, C. Gao, M. Unberath, M. Azizian, D. Stoyanov, L. Maier-Hein, and S. Speidel, "2018 robotic scene segmentation challenge," *CoRR*, vol. abs/2001.11190, 2020.
- [52] W.-Y. Hong, C.-L. Kao, Y.-H. Kuo, J.-R. Wang, W.-L. Chang, and C.-S. Shih, "Cholecseg8k: a semantic segmentation dataset for laparoscopic cholecystectomy based on cholec80," *arXiv preprint arXiv:2012.12453*, 2020.
- [53] D. Sarikaya, J. J. Corso, and K. A. Guru, "Detection and localization of robotic tools in robot-assisted surgery videos using deep neural networks for region proposal and detection," *IEEE Trans. Med. Imaging*, vol. 36, pp. 1542–1549, July 2017.
- [54] A. Jin, S. Yeung, J. Jopling, J. Krause, D. Azagury, A. Milstein, and L. Fei-Fei, "Tool detection and operative skill assessment in surgical videos using region-based convolutional neural networks," in *2018 IEEE Winter Conference on Applications of Computer Vision (WACV)*, pp. 691–699, IEEE, Mar. 2018.
- [55] S. Kondo, "LapFormer: surgical tool detection in laparoscopic surgical video using transformer architecture," *Computer Methods in Biomechanics and Biomedical Engineering: Imaging & Visualization*, vol. 9, pp. 302–307, May 2021.
- [56] D. Bouget, M. Allan, D. Stoyanov, and P. Jannin, "Vision-based and marker-less surgical tool detection and tracking: a review of the literature," *Medical image analysis*, vol. 35, pp. 633–654, 2017.
- [57] S. Speidel, M. Delles, C. Gutt, and R. Dillmann, "Tracking of instruments in minimally invasive surgery for surgical skill analysis," in *Medical Imaging and Augmented Reality: Third International Workshop, Shanghai, China, August 17-18, 2006 Proceedings 3*, pp. 148–155, Springer, 2006.
- [58] Z. Zhao, S. Voros, Y. Weng, F. Chang, and R. Li, "Tracking-by-detection of surgical instruments in minimally invasive surgery via the convolutional neural network deep learning-based method," *Computer Assisted Surgery*, vol. 22, no. sup1, pp. 26–35, 2017.
- [59] N. Padoy, T. Blum, S.-A. Ahmadi, H. Feussner, M.-O. Berger, and N. Navab, "Statistical modeling and recognition of surgical workflow," *Medical image analysis*, vol. 16, no. 3, pp. 632–641, 2012.
- [60] N. A. Jalal, T. A. Alshirbaji, and K. Möller, "Predicting surgical phases using cnn-narx neural network," *Current Directions in Biomedical Engineering*, vol. 5, no. 1, pp. 405–407, 2019.
- [61] Y. Ban, G. Rosman, J. A. Eckhoff, T. M. Ward, D. A. Hashimoto, T. Kondo, H. Iwaki, O. R. Meireles, and D. Rus, "Supr-gan: Surgical prediction gan for event anticipation in laparoscopic and robotic surgery," *IEEE Robotics and Automation Letters*, vol. 7, no. 2, pp. 5741–5748, 2022.
- [62] L. Yin, Y. Ban, J. Eckhoff, O. Meireles, D. Rus, and G. Rosman, "Hypergraph-transformer (hgt) for interactive event prediction in laparoscopic and robotic surgery," *arXiv preprint arXiv:2402.01974*, 2024.
- [63] H. Liu, E. Zhang, J. Wu, M. Hong, and Y. Jin, "Surgical SAM 2: Real-time segment anything in surgical video by efficient frame pruning," *arXiv preprint arXiv:2408.07931*, 2024.
- [64] T. M. Cover and J. A. Thomas, *Elements of Information Theory 2nd Edition (Wiley Series in Telecommunications and Signal Processing)*. Wiley-Interscience, 2 ed., July 2006.
- [65] K. He, X. Zhang, S. Ren, and J. Sun, "Deep residual learning for image recognition," in *Proceedings of the IEEE conference on computer vision and pattern recognition*, pp. 770–778, 2016.
- [66] G. Rosman, Y. Wang, X.-C. Tai, R. Kimmel, and A. M. Bruckstein, "Fast regularization of matrix-valued images," in *Efficient Algorithms for Global Optimization Methods in Computer Vision: International Dagstuhl Seminar, Dagstuhl Castle, Germany, November 20-25, 2011, Revised Selected Papers*, pp. 19–43, Springer, 2014.
- [67] E. T. Jaynes, "Information theory and statistical mechanics," *Physical review*, 1957.
- [68] T. Jain, C. Lennan, Z. John, and D. Tran, "Imagededup." <https://github.com/idealo/imagededup>, 2019.
- [69] J. Wang, K. C. Chan, and C. C. Loy, "Exploring CLIP for assessing the look and feel of images," in AAAI, pp. 2555–2563, 2023.
- [70] A. P. Twinanda, S. Shehata, D. Mutter, J. Marescaux, M. de Mathelin, and N. Padoy, "EndoNet: A deep architecture for recognition tasks on laparoscopic videos," *IEEE Trans. Med. Imaging*, vol. 36, pp. 86–97, Jan. 2017.
- [71] J. Yoon, J. Lee, S. Heo, H. Yu, J. Lim, C. H. Song, S. Hong, S. Hong, B. Park, S. Park, et al., "hsdb-instrument: Instrument localization database for laparoscopic and robotic surgeries," in *Medical Image Computing and Computer Assisted Intervention—MICCAI 2021: 24th International Conference, Strasbourg, France, September 27–October 1, 2021, Proceedings, Part IV 24*, pp. 393–402, Springer, 2021.
- [72] L. Maier-Hein, M. Wagner, T. Ross, A. Reinke, S. Bodenstedt, P. M. Full, H. Hempe, D. Mindroc-Filimon, P. Scholz, T. N. Tran, et al., "Heidelberg colorectal data set for surgical data science in the sensor operating room," *Scientific data*, vol. 8, no. 1, p. 101, 2021.
- [73] M. Carstens, F. M. Rinner, S. Bodenstedt, A. C. Jenke, J. Weitz, M. Distler, S. Speidel, and F. R. Kolbinger, "The dresden surgical anatomy dataset for abdominal organ segmentation in surgical data science," *Scientific Data*, vol. 10, no. 1, pp. 1–8, 2023.
- [74] A. Leibetseder, S. Petscharnig, M. J. Primus, S. Kletz, B. Münzer, K. Schoeffmann, and J. Keckstein, "Lapgyn4: a dataset for 4 automatic content analysis problems in the domain of laparoscopic gynecology," in *Proceedings of the 9th ACM multimedia systems conference*, pp. 357–362, 2018.
- [75] K. Schoeffmann, H. Husslein, S. Kletz, S. Petscharnig, B. Muenzer, and C. Beecks, "Video retrieval in laparoscopic video recordings with dynamic content descriptors," *Multimedia Tools and Applications*, vol. 77, pp. 16813–16832, 2018.
- [76] A. Leibetseder, S. Kletz, K. Schoeffmann, S. Keckstein, and J. Keckstein, "Glenda: gynecologic laparoscopy endometriosis dataset," in *International Conference on Multimedia Modeling*, pp. 439–450, Springer, 2019.
- [77] V. S. Bawa, G. Singh, F. KapingA, I. Skarga-Bandurova, E. Oleari, A. Leporini, C. Landolfo, P. Zhao, X. Xiang, G. Luo, et al., "The saras endoscopic surgeon action detection (esad) dataset: Challenges and methods," *arXiv preprint arXiv:2104.03178*, 2021.
- [78] A. P. Twinanda, *Vision-based approaches for surgical activity recognition using laparoscopic and RBGD videos*. PhD thesis, University of Strasbourg, Strasbourg, France, Jan. 2017.

- [79] Y. Jin, H. Li, Q. Dou, H. Chen, J. Qin, C.-W. Fu, and P.-A. Heng, "Multi-task recurrent convolutional network with correlation loss for surgical video analysis," *Med. Image Anal.*, vol. 59, p. 101572, Jan. 2020.
- [80] A. P. Twinanda, D. Mutter, J. Marescaux, M. de Mathelin, and N. Padoy, "Single- and multi-task architectures for surgical workflow challenge at M2CAI 2016," *arXiv [cs.CV]*, Oct. 2016.
- [81] Y. Jin, Q. Dou, H. Chen, L. Yu, J. Qin, C.-W. Fu, and P.-A. Heng, "SV-RCNet: Workflow recognition from surgical videos using recurrent convolutional network," *IEEE Trans. Med. Imaging*, vol. 37, pp. 1114–1126, May 2018.
- [82] T. Czempiel, M. Paschali, M. Keicher, W. Simson, H. Feussner, S. T. Kim, and N. Navab, "TeCNO: Surgical phase recognition with multi-stage temporal convolutional networks," in *Medical Image Computing and Computer Assisted Intervention – MICCAI 2020*, pp. 343–352, Springer International Publishing, 2020.
- [83] X. Gao, Y. Jin, Y. Long, Q. Dou, and P.-A. Heng, "Trans-SVNet: Accurate phase recognition from surgical videos via hybrid embedding aggregation transformer," in *Medical Image Computing and Computer Assisted Intervention – MICCAI 2021*, pp. 593–603, Springer International Publishing, 2021.
- [84] Y. Liu, M. Boels, L. C. Garcia-Peraza-Herrera, T. Vercauteren, P. Dasgupta, A. Granados, and S. Ourselin, "LoViT: Long video transformer for surgical phase recognition," *Med. Image Anal.*, vol. 99, p. 103366, Oct. 2024.
- [85] S. Yang, L. Luo, Q. Wang, and H. Chen, "Surgformer: Surgical transformer with hierarchical temporal attention for surgical phase recognition," in *International Conference on Medical Image Computing and Computer-Assisted Intervention*, pp. 606–616, Springer, 2024.
- [86] C. I. Nwoye, D. Alapatt, T. Yu, A. Vardazaryan, F. Xia, Z. Zhao, T. Xia, F. Jia, Y. Yang, H. Wang, D. Yu, G. Zheng, X. Duan, N. Getty, R. Sanchez-Matilla, M. Robu, L. Zhang, H. Chen, J. Wang, L. Wang, B. Zhang, B. Gerats, S. Raviteja, R. Sathish, R. Tao, S. Kondo, W. Pang, H. Ren, J. R. Abbing, M. H. Sarhan, S. Bodenstedt, N. Bhasker, B. Oliveira, H. R. Torres, L. Ling, F. Gaida, T. Czempiel, J. L. Vilaça, P. Morais, J. Fonseca, R. M. Egging, I. N. Wijma, C. Qian, G. Bian, Z. Li, V. Balasubramanian, D. Sheet, I. Luengo, Y. Zhu, S. Ding, J.-A. Aschenbrenner, N. E. van der Kar, M. Xu, M. Islam, L. Seenivasan, A. Jenke, D. Stoyanov, D. Mutter, P. Mascagni, B. Seeliger, C. Gonzalez, and N. Padoy, "CholecTriplet2021: A benchmark challenge for surgical action triplet recognition," *Med. Image Anal.*, vol. 86, p. 102803, May 2023.
- [87] C. I. Nwoye, C. Gonzalez, T. Yu, P. Mascagni, D. Mutter, J. Marescaux, and N. Padoy, "Recognition of instrument-tissue interactions in endoscopic videos via action triplets," in *Medical Image Computing and Computer Assisted Intervention – MICCAI 2020*, pp. 364–374, Springer International Publishing, 2020.
- [88] C. I. Nwoye, T. Yu, C. Gonzalez, B. Seeliger, P. Mascagni, D. Mutter, J. Marescaux, and N. Padoy, "Rendezvous: Attention mechanisms for the recognition of surgical action triplets in endoscopic videos," *Med. Image Anal.*, vol. 78, p. 102433, May 2022.
- [89] Y. Ban, J. A. Eckhoff, T. M. Ward, D. A. Hashimoto, O. R. Meireles, D. Rus, and G. Rosman, "Concept graph neural networks for surgical video understanding," *IEEE Trans. Med. Imaging*, vol. PP, July 2023.
- [90] S. Sharma, C. I. Nwoye, D. Mutter, and N. Padoy, "Rendezvous in time: an attention-based temporal fusion approach for surgical triplet recognition," *Int. J. Comput. Assist. Radiol. Surg.*, vol. 18, pp. 1053–1059, June 2023.
- [91] Y. Li, B. Bai, and F. Jia, "Parameter-efficient framework for surgical action triplet recognition," *International Journal of Computer Assisted Radiology and Surgery*, vol. 19, no. 7, pp. 1291–1299, 2024.
- [92] J. N. Paranjape, N. G. Nair, S. Sikder, S. S. Vedula, and V. M. Patel, "AdaptiveSAM: Towards efficient tuning of SAM for surgical scene segmentation," in *Medical Image Understanding and Analysis*, Lecture notes in computer science, pp. 187–201, Cham: Springer Nature Switzerland, 2024.
- [93] J. M. J. Valanarasu, P. Oza, I. Hacıhaliloglu, and V. M. Patel, "Medical transformer: Gated axial-attention for medical image segmentation," in *Medical Image Computing and Computer Assisted Intervention – MICCAI 2021*, pp. 36–46, Springer International Publishing, 2021.
- [94] J. Chen, Y. Lu, Q. Yu, X. Luo, E. Adeli, Y. Wang, L. Lu, A. L. Yuille, and Y. Zhou, "TransUNet: Transformers make strong encoders for medical image segmentation," *arXiv [cs.CV]*, Feb. 2021.
- [95] L.-C. Chen, Y. Zhu, G. Papandreou, F. Schroff, and H. Adam, "Encoder-decoder with atrous separable convolution for semantic image segmentation," *arXiv [cs.CV]*, Feb. 2018.
- [96] A. Hatamizadeh, Y. Tang, V. Nath, D. Yang, A. Myronenko, B. Landman, H. R. Roth, and D. Xu, "UNETR: Transformers for 3D medical image segmentation," in *2022 IEEE/CVF Winter Conference on Applications of Computer Vision (WACV)*, pp. 574–584, IEEE, Jan. 2022.
- [97] F. Isensee, P. F. Jaeger, S. A. Kohl, J. Petersen, and K. H. Maier-Hein, "nnU-net: a self-configuring method for deep learning-based biomedical image segmentation," *Nature methods*, vol. 18, no. 2, pp. 203–211, 2021.
- [98] Z. Zhou, M. M. R. Siddiquee, N. Tajbakhsh, and J. Liang, "UNet++: A nested U-net architecture for medical image segmentation," *Deep Learn. Med. Image Anal. Multimodal Learn. Clin. Decis. Support*, vol. 11045, pp. 3–11, Sept. 2018.
- [99] O. Ronneberger, P. Fischer, and T. Brox, "U-net: Convolutional networks for biomedical image segmentation," in *Lecture Notes in Computer Science*, Lecture notes in computer science, pp. 234–241, Cham: Springer International Publishing, 2015.
- [100] K. Zhang and D. Liu, "Customized segment anything model for medical image segmentation," *arXiv [cs.CV]*, Apr. 2023.
- [101] E. J. Hu, Y. Shen, P. Wallis, Z. Allen-Zhu, Y. Li, S. Wang, L. Wang, and W. Chen, "LoRA: Low-rank adaptation of large language models," *arXiv [cs.CL]*, June 2021.
- [102] J. N. Paranjape, S. Sikder, S. S. Vedula, and V. M. Patel, "S-SAM: SVD-based fine-tuning of segment anything model for medical image segmentation," *arXiv [cs.CV]*, Aug. 2024.
- [103] M. A. Jamal and O. Mohareri, "Rethinking RGB-D fusion for semantic segmentation in surgical datasets," *arXiv [cs.CV]*, July 2024.
- [104] Y. Zhou, H. Badger, M. Read, J. Bailey, and C. E. Davey, "DDA: Dimensionality driven augmentation search for contrastive learning in laparoscopic surgery," *arXiv [cs.CV]*, June 2024.
- [105] M. Sheng, J. Fan, D. Liu, R. Kikinis, and W. Cai, "Revisiting surgical instrument segmentation without human intervention: A graph partitioning view," *arXiv [cs.CV]*, Aug. 2024.
- [106] Y. Tian, G. Pang, F. Liu, Y. Liu, C. Wang, Y. Chen, J. Verjans, and G. Carneiro, "Contrastive transformer-based multiple instance learning for weakly supervised polyp frame detection," in *International Conference on Medical Image Computing and Computer-Assisted Intervention*, pp. 88–98, Springer, 2022.
- [107] J. Park, J. Lee, I.-J. Kim, and K. Sohn, "Probabilistic representations for video contrastive learning," in *Proceedings of the IEEE/CVF conference on computer vision and pattern recognition*, pp. 14711–14721, 2022.
- [108] R. Qian, S. Ding, X. Liu, and D. Lin, "Static and dynamic concepts for self-supervised video representation learning," in *European conference on computer vision*, pp. 145–164, Springer, 2022.
- [109] J. Pan, Z. Lin, X. Zhu, J. Shao, and H. L. ST-Adapter, "Parameter-efficient image-to-video transfer learning for action recognition," *Preprint at https://arxiv.org/abs/2206.13559*, 2022.
- [110] A. Dosovitskiy, L. Beyer, A. Kolesnikov, D. Weissenborn, X. Zhai, T. Unterthiner, M. Dehghani, M. Minderer, G. Heigold, S. Gelly, J. Uszkoreit, and N. Houlsby, "An image is worth 16x16 words: Transformers for image recognition at scale," *arXiv [cs.CV]*, Oct. 2020.
- [111] J. A. Eckhoff, Y. Ban, G. Rosman, D. T. Müller, D. A. Hashimoto, E. Witkowski, B. Babic, D. Rus, C. Bruns, H. F. Fuchs, and O. Meireles, "TEsoNet: knowledge transfer in surgical phase recognition from laparoscopic sleeve gastrectomy to the laparoscopic part of Ivor-Lewis esophagectomy," *Surg. Endosc.*, vol. 37, pp. 4040–4053, May 2023.
- [112] C. R. Johnson and R. A. Horn, *Matrix analysis*. Cambridge university press Cambridge, 1985.